IEEE Access
Multidisciplinary | Rapid Review | Open Access Journal

Date of publication xxxx 00, 0000, date of current version xxxx 00, 0000.

Digital Object Identifier 10.1109/ACCESS.2022.Doi Number

Synthetic Aperture Radar aboard an Unmanned Aerial System for detecting Foreign Object Debris on airport runways

Lapo Miccinesi[1], (Member, IEEE), Alessandra Beni[1], (Member, IEEE), Luca Bigazzi[1] and Massimiliano Pieraccini[1], (Member, IEEE)

[1]Department of Information Engineering (DINFO), University of Florence, 50139 Firenze Italy

Corresponding author: Lapo Miccinesi (e-mail: lapo.miccinesi@unifi.it).

This work was founded by European Union – NextGenerationEU under the project POCARNO22 of the National Recovery and Resilience Plan (NRRP), Mission 1 – Component 2 – Investment 6.

ABSTRACT The detection of foreign object debris (FOD) is a critical safety issue in airport operations. Nowadays, the most advanced detection systems are high frequency radars installed along the runway. In this article, the authors propose a synthetic aperture radar (SAR) aboard a small unmanned aerial system (UAS), a quadcopter, flying sideways over the runway as FOD detection system. This solution can operate during the daily airport operations and does not require permanent installations near the runways. To focus SAR images, an accurate knowledge of the platform position is needed. So, the hardest challenge in SAR imaging with UAS is an effective mitigation and compensation of uncontrolled movements. For this reason, a specific back propagation algorithm was developed. The FOD detection technique was tested in a general aviation airfield (Serristori, Arezzo, Italy) and in two Italian commercial airports: Milan Linate Airport (LIN), Olbia Costa Smeralda Airport (OLB).

INDEX TERMS Airport runway, foreign object debris (FOD), synthetic aperture radar (SAR), unmanned aerial system (UAS), UAS-borne SAR

I. INTRODUCTION

In recent years, many attempts have been made to increase safety in airport areas. The detection of foreign object debris (FOD) of various sizes, which might interfere with aircraft take-off and landing, has received special attention, especially since the well-known Concorde catastrophe that occurred at Charles de Gaulle airport in Paris on July 25, 2000. All 109 people on board, as well as four people on the ground, perished in the catastrophe, which occurred shortly after take-off. A metal strip that was on the runway during take-off caused a tire to shatter, which led to the deadly tragedy.

Flight safety agencies have established standards for the risk assessment in relation to FOD detection and FOD events. For example, the European Union Aviation Safety Agency (EASA) has provided an airport risk assessment tool [1]. This tool requires periodic inspection of the air operations area (AOA), especially for runways and taxiways. The Federal Aviation Administration (FAA) of the United States, additionally, has defined a standard procedure for testing the FOD detection and identification routines [2], [3]. These standards require airport operators to choose the appropriate method for FOD inspection. Currently, the most used method is a visual human inspection, a slow method that requires a large deployment of trained workforce.

In the last years, the development of specific technical solutions has received great attention from the scientific community, business organizations, and aviation authorities [4], [5], [6]. Automatic FOD detection, conducted using cutting-edge technologies, promises to be more effective, fast, and economic than visual human AOA screening.

High resolution vision systems have been used to detect FOD [7], [8], [9], also aboard unmanned aerial systems (UAS) [10], [11]. Unfortunately, optical systems present limited detection capabilities in severe light conditions (dawn, dusk, night, fog, rain).

Alternatively, the radar-based solutions enable all-day, all-weather detection capabilities. Fixed radar installations

near the runway have been proposed and evaluated in [12], [13], [14], [15], [16]. The most advanced systems use multiple sensors installed close to the runway to achieve wider coverage [17], [18], [19], [20]. Since the radar cross-section of the targets strongly depends on the radar line of sight, Yonemoto et al. [18], [21] proposed a multi-monostatic and a bistatic system for increasing the detection probability.

Another technology proposed is a millimetre-wave radar system mounted on the roof of a vehicle [22]. This system scans the pavement below, while the vehicle is moving forward. The system turns out in a large structure which is mounted on a pickup.

Recently, ground-based synthetic aperture radars (GBSARs) have also been proposed for FOD detection: both in linear configuration [23], and in the Arc-SAR configuration [24] to cover a wider field of view.

In this article a W-band SAR aboard a small UAS (a quadcopter) for FOD detection is proposed. The UAS flies sideways over the runway while the radar operates in strip-map modality as shown in Fig. 1. This procedure does not occupy the runway. Therefore, it can be used when the airport is operational, but for safety reason it could not be used during take-off or landing of an airplane. Moreover, it allows to obtain almost constant spatial resolution along the runway.

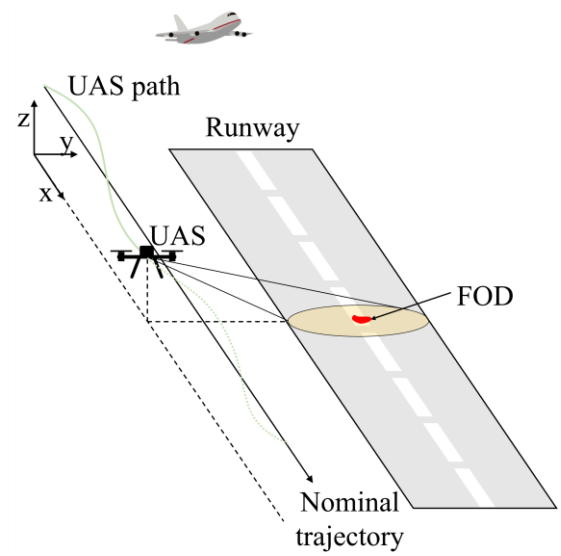

FIGURE 1. Working principle of FOD detection through a radar aboard a UAS.

Today, multicopters are becoming a popular platform for SAR systems [25], [26], [27], [28]. This kind of UAS allows for highly flexible synthetic aperture (SA), and it can be easily deployed without the need fixed installation such as GB-SAR. Unlike satellite and ground-based SAR, multicopter-borne systems are usually subject to uncontrolled movements, caused by external forces, such as wind gusts, which make the image processing more challenging. To properly focus radar data, accurate knowledge of the antenna position and drone attitude is needed. Back-propagation algorithms enable to cope with these problems, provided the knowledge of the UAS position.

Imaging techniques have been studied to perform motion compensation specifically for UAS-based systems [29], [30]. Several works propose autofocusing algorithms to perform high resolution imaging [26], [31]. However, the autofocusing algorithms require a long computational time, since they are usually recursive, and could produce false alarms due to possible focusing artifacts. In most works using UAS-based SAR, back-propagation algorithms are preferred [27], [32], [33], [34].

For the present application, an airborne image processing that considers the platform attitude and position [35] was generalized for UAS applications. The proposed technique was tested in a general aviation airfield (Serristori, Arezzo, Italy) and in two Italian commercial airports: Olbia Costa Smeralda Airport (OLB) and Milan Linate Airport (LIN).

II. FOCUSING ALGORITHM

The SAR images were focused using a back-propagation algorithm based on [35], originally developed for airborne SAR.

The geometry of the UAS-borne SAR acquisition is shown in Fig. 2. In the following we assume that the radar is in $\vec{A}_n$ at the (slow) time t_n. The target to be focused is in $\vec{T}$. The vector $\vec{R}_n(\vec{T})$ represents the position of the target with respect to the radar at the slow time t_n.

$$\vec{R}_n(\vec{T}) = \vec{T} - \vec{A}_n. \quad (1)$$

The module $R_n(\vec{T}) = |R_n(\vec{T})| = |\vec{T} - \vec{A}_n|$ represents the range distance between antennas and the target.

Let us consider a continuous wave frequency modulated (FMCW) transceiver with sawtooth modulation. The acquired echo is a complex matrix E_{nm} whose indexes $n \in \{1,2,\dots N_{sweep}\}$ and $m \in \{1,2,\dots N_{sample}\}$ are related to slow (n) and fast time (m), respectively. N_{sweep} is the number of recorded azimuth samples (along slow time) and N_{sample} is the number of the samples recorded in range direction (along fast time).

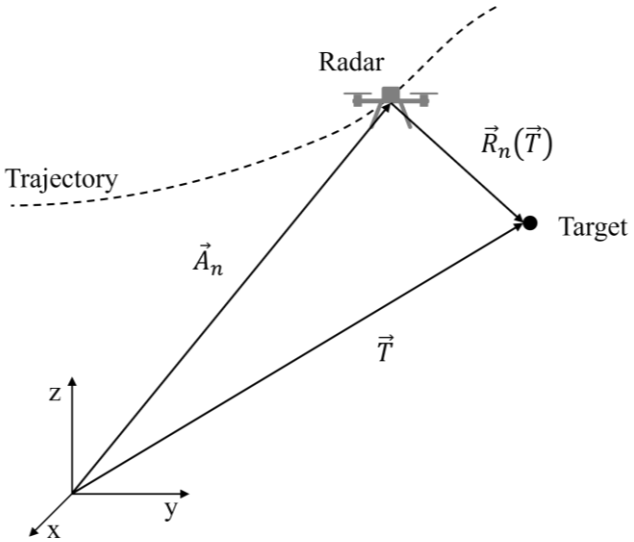

FIGURE 2. **Focusing geometry.**

The radar image $I(\vec{T})$ of target $\vec{T}$ can be retrieved with the back propagation algorithm based on [35], as

$$I(\vec{T}) = \sum_{m=1}^{m=N_{sample}} \sum_{n=k-\frac{K}{2}}^{n=k+\frac{K}{2}} E_{nm} \exp\left[-j\frac{4\pi}{c} f_m R_n(\vec{T})\right] w_m \cdot w_n\left(R_n(\vec{T})\right). \quad (2)$$

Here, k, K are the centre and the length (in samples) of the synthetic aperture (SA), j is the complex unit, w_m is the weight of the range-window, $w_n\left(\mathrm{R_n}\left(\vec{T}\right)\right)$ is the weight of cross-range window, and f_m is the m-frequency given by

$$f_m = f_0 + m\alpha\Delta t, \quad (3)$$

with α the frequency slope of the FM sweep, and Δt the time stamp of analog-to-digital converter (ADC) [36].

The range and cross-range windows are applied to reduce the side lobe level of the image in the two directions. In the following, we use a Kaiser window with β=5. Given the high computational cost of (2), we used the solution described in [37], which uses the fast Fourier transform in the range direction and an interpolation method to reduce the computational cost.

The computation of (2) requires accurate knowledge of the radar-to-target distance $R_n\left(\vec{T}\right)$, and the definition of the SA length K. The radar-to-target distance $R_n\left(\vec{T}\right)$ depends on the radar position $\vec{A}_n$, which can be retrieved by the navigation data. UAS are usually equipped with inertial measurement units (IMUs) and a real time kinematic global positioning satellite system (GNSS-RTK). In general, data recorded by these sensors are affected by uncertainty and bias. To recover the correct position of the UAS, an estimation method is required, i.e. a filter fusion algorithm [38], or a Kalman filter [39]. In this article, we used a modified version of the complementary double stage filter [40], which uses the acceleration, velocity, and position of several sensors to provide a position estimate. Each data was filtered in the proper operative band, e.g. the acceleration was filtered with high pass filter, while the velocity and the position with a low pass filter.

The SA, K, is limited by the uncertainty and residual bias of the recovered position. Indeed, increasing the SA implies adding noise in the complex term of the exponential in (2). This noise produces a defocusing effect in the final image when the SA is too wide. On the other hand, increasing the SA improves the signal-to-noise ratio (SNR). Therefore, the value of SA is a trade-off between image quality and SNR, and it depends on the measurement conditions.

Equation (2) is implemented considering a focusing grid on the ground, based on the flight trajectory. The geometry is shown in Fig. 3. The x axis is parallel to the average UAS flight direction. For each y position on the grid, the centre of the scan k is identified by the projection of the y coordinate of the trajectory. To reduce the computational cost, we used the same aperture K for the targets with the same x coordinate.

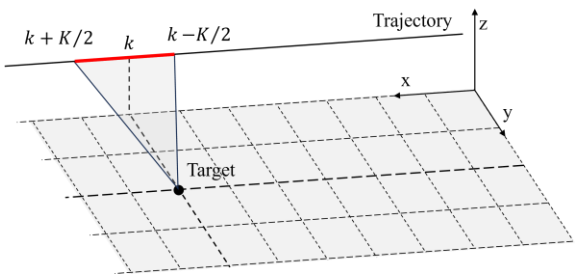

FIGURE 3. **Focusing grid.**

III. THE EQUIPMENT

The payload of the FOD detection system is composed by an onboard computer and a W-band radar. A block scheme of the system is shown in Fig. 4. The onboard computer hosts the Robot Operating System (ROS) [41] which enables the communication with the UAS and the radar. ROS is a software framework which allows to implement and schedule different tasks, e.g. the communication with the UAS or the sensor data acquisition. The use of ROS guarantees independence from the specific hardware used: it allows you to change hardware without changing the structure of the software, but only specific tasks. ROS has been used for recording the telemetry information of the UAS and to trigger the radar measurements. The internal timestamp of ROS was used to synchronize the radar and the UAS telemetry. The radar image was processed in post-processing on a ground computational unit after each flight.

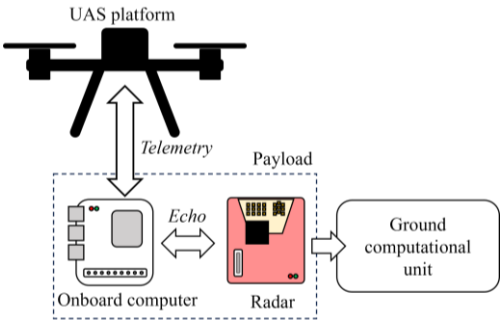

FIGURE 4. **Block scheme of the UAS borne SAR for FOD detection.**

The radar used for FOD detection is an AWR1843BOOST by Texas Instruments [42]. It is a single chip radar designed for automotive purposes. Due to its low weight and low power consumption, it can be employed for UAS applications [36], [43]. During the experiment, the radar provided an FMCW sawtooth signal from 77.124 GHz, with frequency slope [36] $\alpha = 6.2\ MHz/\mu s$, ADC time stamp $\Delta t = 0.105\ \mu s$, and number of frequency samples $N_{sample} = 1024$. The bandwidth is $B = 664.1\ MHz$, which results in a range resolution ($\Delta R = c/(2B)$ [44]) of about $0.23\ m$.

Fig. 5 and Fig. 6 show the equipment aboard a Matrice300RTK by DJI [45] and a PLL418 by Nimbus SRL, property of Techno Sky. The first UAS (Fig. 5) was used during the tests in the controlled environment. The second UAS [46] was used during the tests in real scenarios, because it ensures the safety level required for flying inside AOA. It is also equipped with a remote battery switch and a parachute.

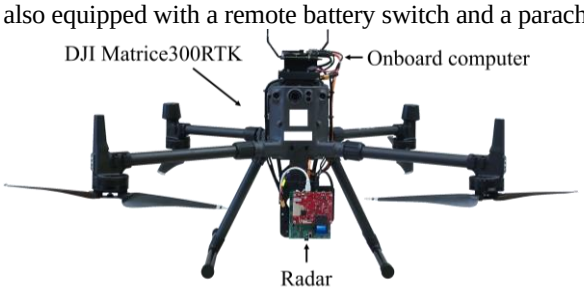

FIGURE 5. **Radar payload aboard a Matrice300RTK by DJI.**

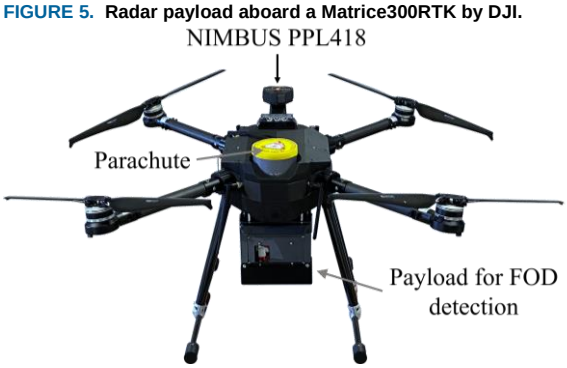

FIGURE 6. **Radar payload aboard a PLL418 by Nimbus SRL.**

IV. EXPERIMENTAL TESTS

A. GENERAL AVIATION AIRFIELD OF SERRISTORI, AREZZO, ITALY

The UAS-borne system was initially tested in a small general aviation airfield (Serristori, Arezzo, Italy). The first test was carried out with a single corner reflector to validate and characterize the focusing process. The corner reflector, $25\ mm$ large, was located on the runway of the airfield as shown in Fig. 7. The runway was $20\ m$ wide. The radar flew at $2\ m$ altitude and $17\ m$ from the corner reflector. The UAS scanned about $15\ m$ of runway at $3\ m/s$ of speed. Radar raw data were processed using (2) with different SA, between $0.5\ m$ and $5\ m$. The quality of the SAR images in terms of point spread function (PSF) at $-10\ dB$, and the SNR, were evaluated.

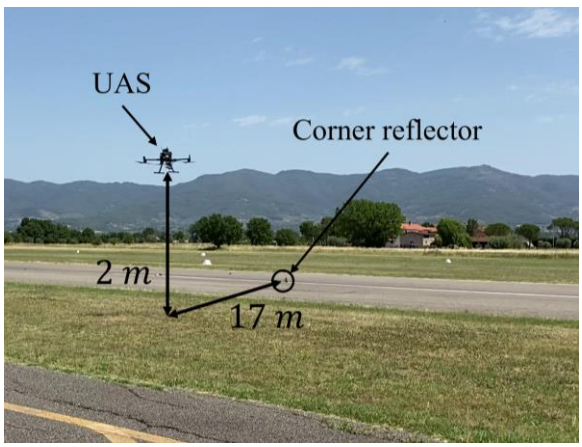

FIGURE 7. **Measurement setup in the general aviation airfield.**

Fig. 8 shows the effect of the SA length on the PSF. The PSF appears of good quality for SA between $0.5\ m$ and $1.5\ m$. Conversely, for SA $= 5\ m$ the target is completely defocused: the peak divides into others of almost the same amplitude. The defocusing effect is related to a not perfect compensation of the antenna position that produces a cumulative effect in the back-propagation algorithm.

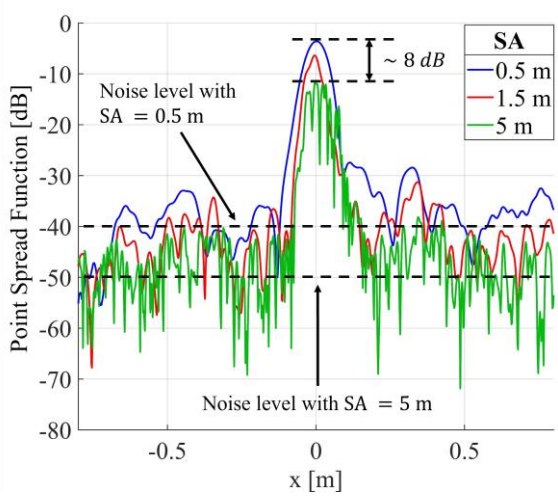

FIGURE 8. **Point spread function (PSF) in terms of SA.**

To better highlight how the SA length affects the image quality, the width of PSF at $-10\,dB$ and the SNR were calculated as functions of SA (Fig. 9 and Fig. 10). Fig. 9 shows the width of PSF calculated at -10 dB respect to the maximum. The PSF width decreases from $0.12\,m$ (for SA $=$ $0.5\,m$) to about $0.08\,m$ (for SA $= 2.5\,m$). Then, for SA wider than $2.5\,m$, the width dramatically increases since the main lobe splits in several peaks.

Fig. 10 shows the SNR as a function of SA. The SNR grows up to SA $\approx 3\,m$; then it remains approximately constant. It can be argued that the optimal value of SA is a trade-off between image quality and SNR. In this specific case, SA = 1 m could be a good choice.

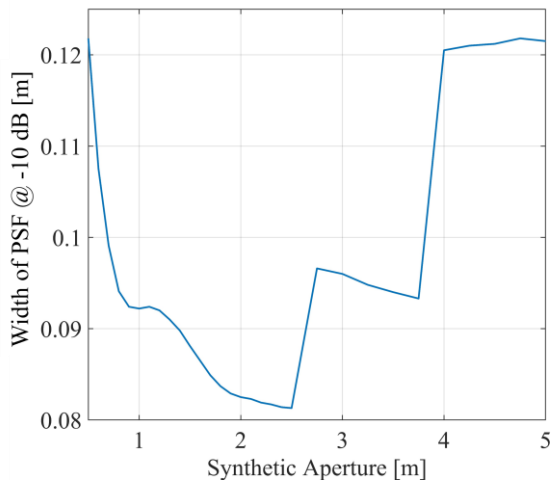

FIGURE 9. **PSF width versus SA.**

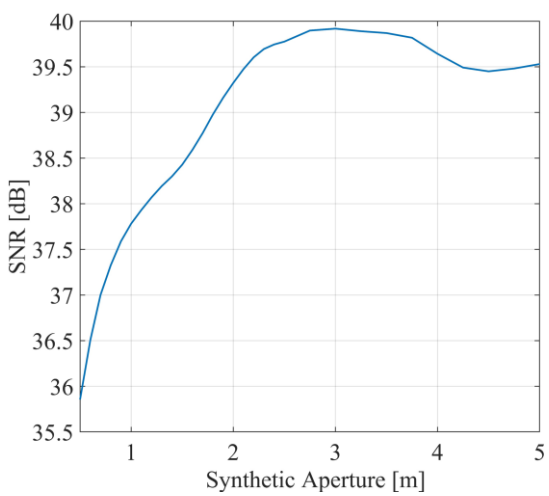

FIGURE 10. **SNR versus SA.**

The capability of the sensor to detect different FODs was tested in the controlled scenario of runway. The asphalt runway was $500\,m$ long and $20\,m$ wide. Eight FODs were positioned along $30\,m$ of the runway, as shown in Fig. 11. The UAS performed a flight scan $50\,m$ long, at $2\,m$ altitude and $17\,m$ away from the centre of the runway.

For this test, FODs with different shape and size have been used. An image and physical size of each FOD are shown in Fig. 12.

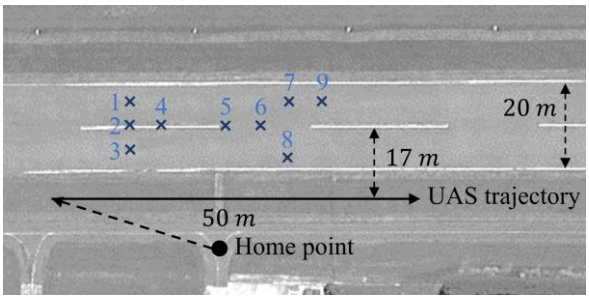

FIGURE 11. **Measurement setup of general aviation airfield scenario.**

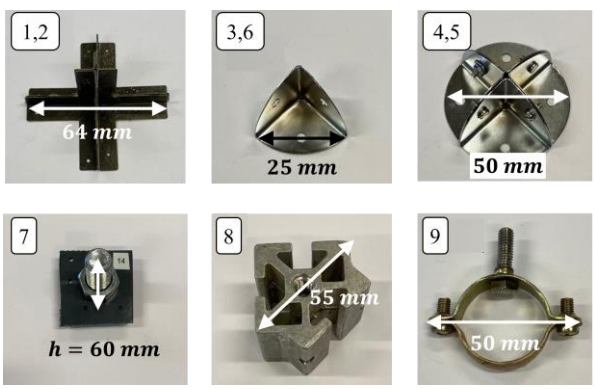

FIGURE 12. **Images of the FODs used during the test at Serristori airfield.**

Fig. 13 shows the radar image obtained using an SA of 1 m. All FODs were successfully detected and appear as well-defined bright spots in the image. The runway edges are also clearly visible at y = 5 m and y = 25 m. They are highlighted by red dashed lines in Fig. 13. There are also two longitudinal reflections at y = 10 m and y = 13 m which correspond to junctions in the asphalt of the runway.

It is important to note the strong clutter signal within $y \approx 10\,m$. This clutter is given by the first reflection of the signal from the ground close to the radar. Therefore, when possible, it may be preferable to fly away (at least 10 m) from the runway to prevent the FOD detection capabilities from being affected by close-range clutter.

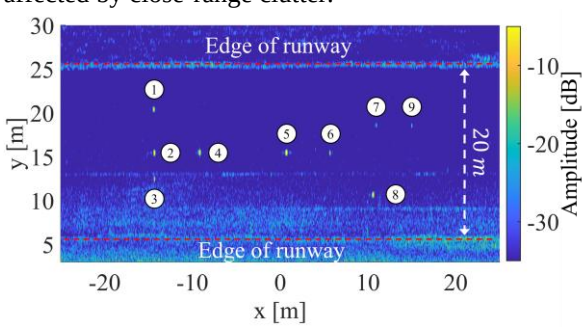

FIGURE 13. **Radar image of general aviation airfield.**

B. MILANO-LINATE AIRPORT (LIN), MILAN, ITALY

A second measurement campaign was performed at the Milano-Linate airport, Italy, to test the technique in a realistic scenario. The tests were performed on the Taxiway Tango of the airport. Fig. 14 shows the measurement setup: the sensor was mounted on board the Techno sky UAS (that is certified for flying in operative commercial airports) and was connected to a ground control laptop trough a Wi-Fi link. The ground control laptop enables and disables the measurement and controls the measurement status. The test was carried out during the night break of airport activities.

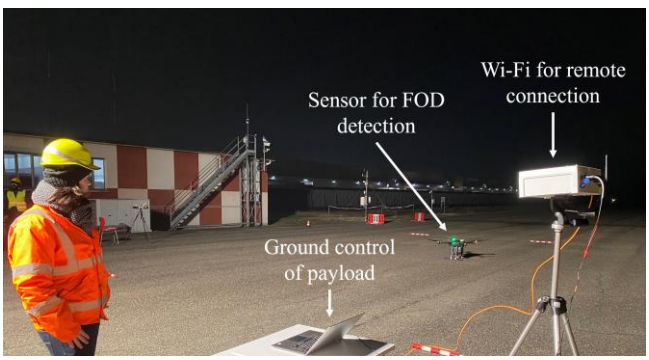

FIGURE 14. **Measurement setup for the inspection of Taxiway Tango of Milano-Linate Airport.**

The FODs were selected according to the FAA guideline [2], [3]. Table I lists the FODs with a brief description and physical dimensions. Pictures of the FODs used are shown in Fig. 15. The FODs were placed on the taxiway as shown in Fig. 16. The taxiway is 60 m wide, the inspected section was about 400 m long. The UAS flew at 3 m altitude and about 10 m from the edge of the investigated area. The taxiway was scanned in both directions to maximize the probability of detection. There was no wind during the flight. In Fig. 16, blue crosses indicate the detected FODs, while the red crosses indicate the undetected ones.

TABLE I
DESCRIPTION OF FOD USED AT LINATE.

ID	Description	Size A [mm]	Size B [mm]
A	Sphere	30	-
B	Cylinder	38	31
C	Wrench	200	-
D	Electric Socket	40	40
E	Distorted metal strip	280	-
F	Fuel cap	86	72
G	Hydraulic line	300	-
H	Cotter pin (safety)	100	-
L	"Chunk" of concrete	100	-
M	Piece of tire	270	180
N	Lug nut	120	-

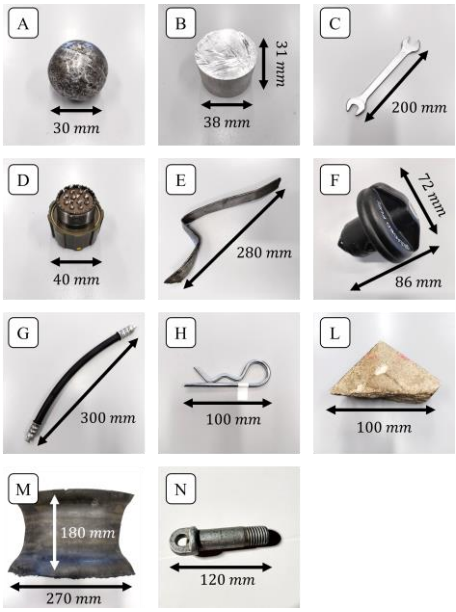

FIGURE 15. **Images of the FODs used during the inspection in Linate selected from FAA document [2], [3].**

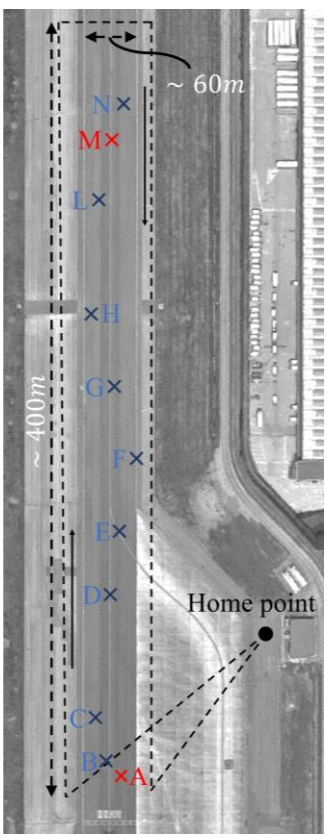

FIGURE 16. **Aerial view of the Taxiway Tango of Milano-Linate Airport.**

The image was focused with an SA = 4 m to increase the SNR. Fig. 17 shows the results for each detected FOD. During this inspection FOD B, C, D, E, F, G, H, L, N were detected. In particular, FOD C and FOD H were detected only during the forward flight, and FOD G was detected only

during the return flight. The other detected FODs were visible in both flights. FOD C is barely visible. FOD A and FOD M were not detected. Probably because the size of FOD A was at the limit of sensor resolution, and the material of FOD M (rubber) is notoriously transparent to the electromagnetic waves.

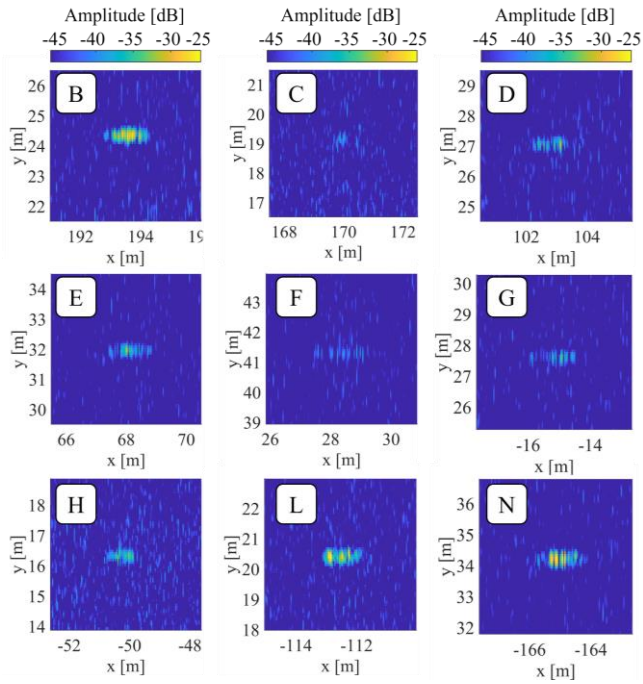

FIGURE 17. Results of the Taxiway Tango of Milano-Linate Airport.

C. OLBIA COSTA SMERALDA AIRPORT (OLB), OLBIA, ITALY

The technique was finally tested on the Taxiway Golf of the Olbia Costa Smeralda Airport using realistic small FODs, found in the Air Operation Area (AOA) by the airport staff. Fig. 18 shows the measurement setup. A further element of difficulty that made the test a sort of worst-case study, was the strong wind. As it can be noticed in the photo, during the inspection at the OLB, there were wind gusts up to 37 km/h.

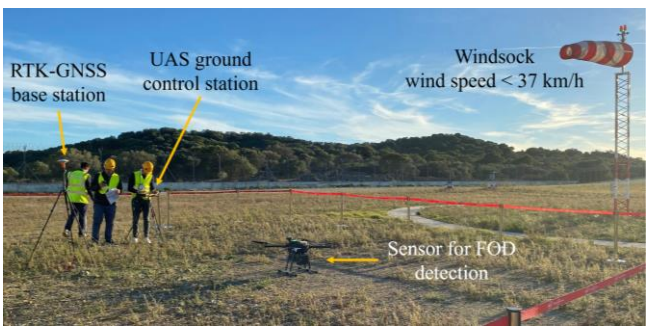

FIGURE 18. Measurement setup during the inspection with realistic FODs in Olbia Costa Smeralda Airport.

Table II lists the selected FODs and provides a brief description and their size. The FODs were made of metal material except for FOD V, which was made of rubber.

A picture of each FOD is reported in Fig. 19. They were placed on the taxiway as shown in Fig. 20. The taxiway is 40 m wide, the scan was about 180 m long. The UAS flew at 2 m altitude and about 5 m from the edge of the taxiway. The sensor scanned both sides of the taxiway.

TABLE II
DESCRIPTION OF FOD USED DURING TAXIWAY INSPECTION.

ID	Description	Size A [mm]	Size B [mm]
I	Cylinder	25	15
II	Bolt	25	-
III	Metallic pin	40	-
IV	Nut	30	-
V	Piece of tire	190	-
VI	Brake component	120	30

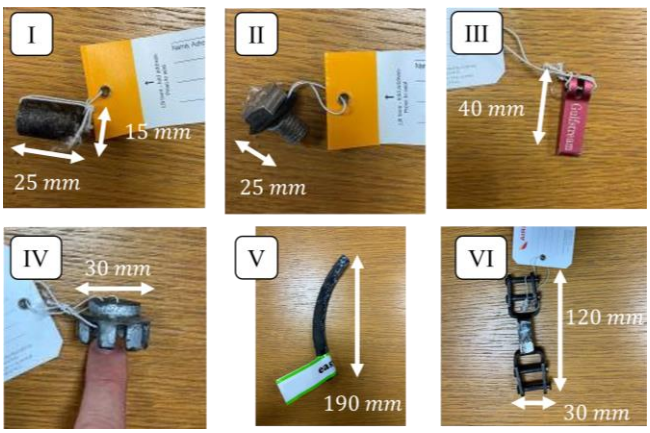

FIGURE 19. Images of the FODs used during the inspection of the Taxiway Golf of Olbia Costa Smeralda Airport.

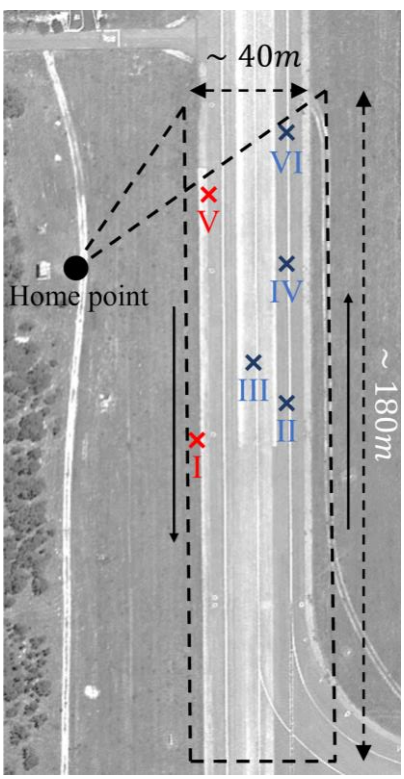

FIGURE 20. Aerial view of the Taxiway Golf of Olbia Costa Smeralda Airport.

In this case, the image was focused with SA $= 1\,m$ because the defocusing effect due to the wind was higher than in the previous cases. The UAS velocity was not constant, and the trajectory significantly deviated from the nominal straight one. Fig. 21 shows the radar image of each detected FOD. FOD II, FOD III, FOD IV, and FOD VI were detected. All these FODs were detected in the forward and return scan.

FOD I and FOD V were not detected during this mission. Regarding FOD V, as already mentioned for the LIN experiment, the material (rubber) is transparent to radar radiation. For what concerns FOD I, it was located close to the edge of the taxiway and the vegetated area. Its signal was probably covered by the clutter given by the vegetated area.

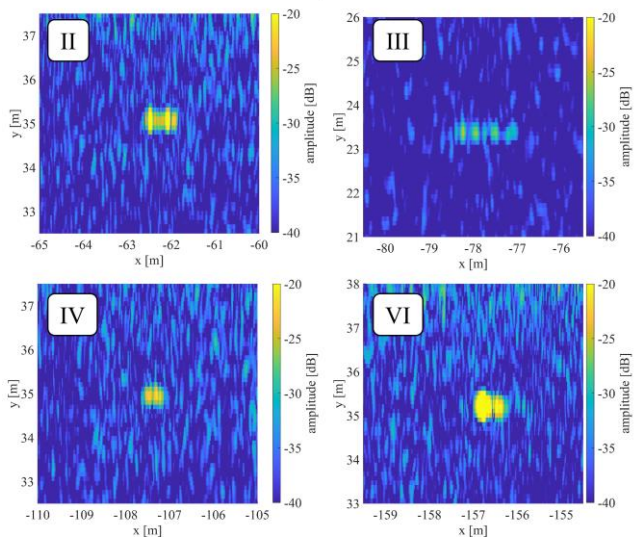

FIGURE 21. Results of the Taxiway Tango of Milano-Linate Airport.

V. CONCLUSIONS

In this article, a UAS-borne W-band SAR system for FOD detection was presented. The system was validated with experimental tests both in controlled and realistic scenarios with different kinds of FODs. The UAS-borne SAR was able to successfully detect FODs of size between 25 – 60 mm, except for rubber or plastic materials.

In conclusion, we can state that the potential of FOD detection through SAR aboard UAS has been successfully demonstrated. Nevertheless, its effective application in operational conditions needs full compliance with the guidelines for FOD detection published by each single national aviation authority. As an example, U.S. Federal Aviation Administration (FAA) prescribes [3] that all FOD removal equipment must be able to demonstrate the ability to collect 90 % of items of a specific list, by a single pass of the equipment at a minimum speed of 25 km/h. Most of the items prescribed by FAA were successfully detected, but the percentage of detection relative to tests presented in this article, was about 81 %. For improving the detection capability, i.e. the SNR, there are several ways: increasing the transmitted power, increasing the antenna gain, improving the flight stability and the motion compensation for increasing the effective SA. Another critical point is the scan speed requirement: 25 km/h. The speed of the UAS during the experimental tests presented in this article was 11 km/h (3 m/s). For a faster acquisition, it is necessary to increase the PRF (from 3.33 kHz to 7.59 kHz) or alternatively to increase the antenna directivity, by increasing its size by a factor of 2.3.

A final word of caution for an operational application of this FOD detection technique is relative to the SA setting. As noticed above, the value of SA is a trade-off between image quality and SNR, and it depends on the measurement conditions, particularly the wind. In the radar images presented in this article, the SA has been set for each single image with a "trial and error" approach. In an operational application, the detection should be finalized in a few minutes after the flight, so a systematic study of correlation between meteorological conditions and optimal SA should be carried out.

ACKNOWLEDGMENT

This work was supported and co-funded by Techno Sky S.r.l., an ENAV company. ENAV S.p.A. is the Italian air navigation service provider. The authors would like to thank the airport operators of Linate airport and Olbia airport for their support. The authors would like to acknowledge the encouragement and support of Claudio Fausto Petrachi of Techno Sky, that from the beginning believed in the potential of this technology. A special thanks to Giuseppe Ramalli of Serristori airfield for his enthusiastic and competent support.

REFERENCES

[1] 'Easy Access Rules for Aerodromes (Regulation (EU) No 139/2014) - Revision from June 2023', EASA. Accessed: Jan. 08, 2024. [Online]. Available: https://www.easa.europa.eu/en/document-library/easy-access-rules/online-publications/easy-access-rules-aerodromes-regulation-eu

[2] 'FAA Foreign Object Debris Program | Federal Aviation Administration'. Accessed: Jan. 10, 2024. [Online]. Available: https://www.faa.gov/airports/airport_safety/fod

[3] Federal Aviation Administration, 'AC 150/5210-24 - Airport Foreign Object Debris (FOD) Management'. Sep. 03, 2010. Accessed: Jan. 10, 2024. [Online]. Available: https://www.faa.gov/airports/resources/advisory_circulars/index.cfm/go/document.current/documentNumber/150_5210-24

[4] D. J. Shephard, P. D. F. Tait, and R. J. King, 'Foreign object detection using radar', in *2000 IEEE Aerospace Conference. Proceedings (Cat. No.00TH8484)*, Mar. 2000, pp. 43–48 vol.6. doi: 10.1109/AERO.2000.877881.

[5] Li Ang, 'Research and Design of an Airfield Runway FOD Detection System Based on WSN', *International Journal of Distributed Sensor Networks*, vol. 9, no. 12, pp. 1–6, Dec. 2013, doi: 10.1155/2013/839586.

[6] Y. Zhongda, L. Mingguang, and C. Xiuquan, 'Research and implementation of FOD detector for airport runway', *IOP Conf. Ser.: Earth Environ. Sci.*, vol. 304, no. 3, p. 032050, Sep. 2019, doi: 10.1088/1755-1315/304/3/032050.

[7] Y. Liu, Y. Li, J. Liu, X. Peng, Y. Zhou, and Y. L. Murphey, 'FOD Detection using DenseNet with Focal Loss of Object Samples for

Airport Runway', in *2018 IEEE Symposium Series on Computational Intelligence (SSCI)*, Nov. 2018, pp. 547–554. doi: 10.1109/SSCI.2018.8628648.

[8] Y. Jing, H. Zheng, C. Lin, W. Zheng, K. Dong, and X. Li, 'Foreign Object Debris Detection for Optical Imaging Sensors Based on Random Forest', *Sensors*, vol. 22, no. 7, Art. no. 7, Jan. 2022, doi: 10.3390/s22072463.

[9] R. A. Amit and C. K. Mohan, 'GeoMask : Foreign Object Debris Instance Segmentation Using Geodesic Representations', in *2022 IEEE Aerospace Conference (AERO)*, Mar. 2022, pp. 1–9. doi: 10.1109/AERO53065.2022.9843628.

[10] A. Parker, F. Gonzalez, and P. Trotter, 'Live Detection of Foreign Object Debris on Runways Detection using Drones and AI', in *2022 IEEE Aerospace Conference (AERO)*, Mar. 2022, pp. 1–13. doi: 10.1109/AERO53065.2022.9843697.

[11] E. Papadopoulos and F. Gonzalez, 'UAV and AI Application for Runway Foreign Object Debris (FOD) Detection', in *2021 IEEE Aerospace Conference (50100)*, Mar. 2021, pp. 1–8. doi: 10.1109/AERO50100.2021.9438489.

[12] P. D. L. Beasley, G. Binns, R. D. Hodges, and R. J. Badley, 'Tarsier/spl R/, a millimetre wave radar for airport runway debris detection', in *First European Radar Conference, 2004. EURAD.*, Oct. 2004, pp. 261–264.

[13] 'Automatic Foreign Object Detection Debris'. Accessed: Jan. 18, 2024. [Online]. Available: https://www.qinetiq.com/en/what-we-do/services-and-products/automatic-foreign-object-debris-detection

[14] M. Ferri, G. Giunta, A. Banelli, and D. Neri, 'Millimetre wave radar applications to airport surface movement control and foreign object detection', in *2009 European Radar Conference (EuRAD)*, Sep. 2009, pp. 437–440.

[15] A. Zeitler, J. Lanteri, C. Pichot, C. Migliaccio, P. Feil, and W. Menzel, 'Folded Reflectarrays With Shaped Beam Pattern for Foreign Object Debris Detection on Runways', *IEEE Transactions on Antennas and Propagation*, vol. 58, no. 9, pp. 3065–3068, Sep. 2010, doi: 10.1109/TAP.2010.2052564.

[16] 'Elva-1'. Accessed: Jan. 18, 2024. [Online]. Available: https://elva-1.com/products/a40155

[17] A. Kohmura, S. Futatsumori, N. Yonemoto, and K. Okada, 'Optical fiber connected millimeter-wave radar for FOD detection on runway', in *2013 European Radar Conference*, Oct. 2013, pp. 41–44.

[18] N. Yonemoto, A. Kohmura, S. Futatsumori, K. Morioka, and N. Kanada, 'Two Dimensional Radar Imaging Algorithm of Bistatic Millimeter Wave Radar for FOD Detection on Runways', in *2018 International Topical Meeting on Microwave Photonics (MWP)*, Oct. 2018, pp. 1–4. doi: 10.1109/MWP.2018.8552847.

[19] S. Futatsumori, K. Morioka, A. Kohmura, and N. Yonemoto, 'Long-Distance Coherent Signal Transmission and Reception of Optically-Connected 96 GHz Millimeter-Wave Radar System for Runway Foreign Object Debris Detection', in *2019 44th International Conference on Infrared, Millimeter, and Terahertz Waves (IRMMW-THz)*, Sep. 2019, pp. 1–2. doi: 10.1109/IRMMW-THz.2019.8874480.

[20] J. Wang, X. Geng, and S. Wei, 'Airport Runway FOD Detection System Based on 77GHz Millimeter Wave Radar Sensor', in *2019 IEEE International Conference on Integrated Circuits, Technologies and Applications (ICTA)*, Nov. 2019, pp. 140–143. doi: 10.1109/ICTA48799.2019.9012911.

[21] N. Yonemoto, S. Futatsumori, A. Kohmura, K. Morioka, N. Kanada, and N. Sakamoto, 'Bi-static Millimeter Wave Radar Connected by Radio over Fiber for FOD Detection on Runways', in *2019 IEEE Conference on Antenna Measurements & Applications (CAMA)*, Oct. 2019, pp. 147–150. doi: 10.1109/CAMA47423.2019.8959741.

[22] 'FOD FInder'. Accessed: Jan. 18, 2024. [Online]. Available: http://www.trexenterprises.com/fodfinderSite/pages/fodfinder.html

[23] M. Sato, '2-D and 3-D near range SAR imaging', in *2017 IEEE Conference on Antenna Measurements & Applications (CAMA)*, Dec. 2017, pp. 157–160. doi: 10.1109/CAMA.2017.8273387.

[24] Y. Wang, Q. Song, J. Wang, and H. Yu, 'Airport Runway Foreign Object Debris Detection System Based on Arc-Scanning SAR Technology', *IEEE Transactions on Geoscience and Remote Sensing*, vol. 60, pp. 1–16, 2022, doi: 10.1109/TGRS.2022.3143243.

[25] L. Miccinesi, A. Beni, and M. Pieraccini, 'UAS-Borne Radar for Remote Sensing: A Review', *Electronics*, vol. 11, no. 20, Art. no. 20, Jan. 2022, doi: 10.3390/electronics11203324.

[26] A. Bekar, M. Antoniou, and C. J. Baker, 'Low-Cost, High-Resolution, Drone-Borne SAR Imaging', *IEEE Transactions on Geoscience and Remote Sensing*, vol. 60, pp. 1–11, 2022, doi: 10.1109/TGRS.2021.3085235.

[27] G. Oré *et al.*, 'Predicting Sugarcane Harvest Date and Productivity with a Drone-Borne Tri-Band SAR', *Remote Sensing*, vol. 14, no. 7, Art. no. 7, Jan. 2022, doi: 10.3390/rs14071734.

[28] A. Carpenter, J. A. Lawrence, R. Ghail, and P. J. Mason, 'The Development of Copper Clad Laminate Horn Antennas for Drone Interferometric Synthetic Aperture Radar', *Drones*, vol. 7, no. 3, Art. no. 3, Mar. 2023, doi: 10.3390/drones7030215.

[29] P. Stockel, P. Wallrath, R. Herschel, and N. Pohl, 'Motion Compensation in Six Degrees of Freedom for a MIMO Radar Mounted on a Hovering UAV', *IEEE Transactions on Aerospace and Electronic Systems*, vol. 59, no. 5, pp. 5791–5801, Oct. 2023, doi: 10.1109/TAES.2023.3266181.

[30] Z. Lv, F. Li, X. Qiu, and C. Ding, 'Effects of Motion Compensation Residual Error and Polarization Distortion on UAV-Borne PolInSAR', *Remote Sensing*, vol. 13, no. 4, Art. no. 4, Jan. 2021, doi: 10.3390/rs13040618.

[31] Z. Ding *et al.*, 'An Autofocus Back Projection Algorithm for GEO SAR Based on Minimum Entropy', *IEEE Transactions on Geoscience and Remote Sensing*, vol. 60, pp. 1–14, 2022, doi: 10.1109/TGRS.2022.3164922.

[32] M. Lort, A. Aguasca, C. López-Martínez, and T. M. Marín, 'Initial Evaluation of SAR Capabilities in UAV Multicopter Platforms', *IEEE Journal of Selected Topics in Applied Earth Observations and Remote Sensing*, vol. 11, no. 1, pp. 127–140, Jan. 2018, doi: 10.1109/JSTARS.2017.2752418.

[33] L. Moreira *et al.*, 'A Drone-borne Multiband DInSAR: Results and Applications', in *2019 IEEE Radar Conference (RadarConf)*, Apr. 2019, pp. 1–6. doi: 10.1109/RADAR.2019.8835653.

[34] O. Frey, C. L. Werner, and R. Coscione, 'Car-borne and UAV-borne mobile mapping of surface displacements with a compact repeat-pass interferometric SAR system at L-band', in *IGARSS 2019 - 2019 IEEE International Geoscience and Remote Sensing Symposium*, Jul. 2019, pp. 274–277. doi: 10.1109/IGARSS.2019.8897827.

[35] P. Berardino, A. Natale, C. Esposito, R. Lanari, and S. Perna, 'On the Time-Domain Airborne SAR Focusing in the Presence of Strong Azimuth Variations of the Squint Angle', *IEEE Transactions on Geoscience and Remote Sensing*, vol. 61, pp. 1–18, 2023, doi: 10.1109/TGRS.2023.3289593.

[36] L. Miccinesi *et al.*, 'Geo-Referenced Mapping through an Anti-Collision Radar Aboard an Unmanned Aerial System', *Drones*, vol. 6, no. 3, Art. no. 3, Mar. 2022, doi: 10.3390/drones6030072.

[37] M. Pieraccini and L. Miccinesi, 'ArcSAR: Theory, Simulations, and Experimental Verification', *IEEE Transactions on Microwave Theory and Techniques*, vol. 65, no. 1, pp. 293–301, Jan. 2017, doi: 10.1109/TMTT.2016.2613926.

[38] P. Pierleoni, A. Belli, L. Palma, L. Pernini, and S. Valenti, 'An accurate device for real-time altitude estimation using data fusion algorithms', in *2014 IEEE/ASME 10th International Conference on Mechatronic and Embedded Systems and Applications (MESA)*, Sep. 2014, pp. 1–5. doi: 10.1109/MESA.2014.6935583.

[39] 'UAV Position Estimation and Collision Avoidance Using the Extended Kalman Filter | IEEE Journals & Magazine | IEEE Xplore'. Accessed: Jan. 10, 2024. [Online]. Available: https://ieeexplore.ieee.org/abstract/document/6422418

[40] P. Marantos, Y. Koveos, and K. J. Kyriakopoulos, 'UAV State Estimation Using Adaptive Complementary Filters', *IEEE Transactions on Control Systems Technology*, vol. 24, no. 4, pp. 1214–1226, Jul. 2016, doi: 10.1109/TCST.2015.2480012.

[41] A. Koubaa, Ed., *Robot Operating System (ROS)*, vol. 625. in Studies in Computational Intelligence, vol. 625. Cham: Springer International Publishing, 2016. doi: 10.1007/978-3-319-26054-9.

[42] 'AWR1843BOOST Evaluation board | TI.com'. Accessed: Jan. 01, 2024. [Online]. Available: https://www.ti.com/tool/AWR1843BOOST

[43] L. Bigazzi, L. Miccinesi, E. Boni, M. Basso, T. Consumi, and M. Pieraccini, 'Fast Obstacle Detection System for UAS Based on Complementary Use of Radar and Stereoscopic Camera', *Drones*, vol. 6, no. 11, Art. no. 11, Nov. 2022, doi: 10.3390/drones6110361.
[44] M. Pieraccini and L. Miccinesi, 'Ground-based radar interferometry: A bibliographic review', *Remote Sensing*, vol. 11, no. 9, 2019, doi: 10.3390/rs11091029.
[45] 'Matrice 300 RTK', DJI. Accessed: Jan. 01, 2024. [Online]. Available: https://www.dji.com/matrice-300?site=brandsite&from=nav
[46] 'Nimbus - QUADCOPTER', Nimbus.aero. Accessed: Jul. 16, 2024. [Online]. Available: https://www.nimbus.aero/products

LAPO MICCINESI (Member IEEE) received the B.S. degree in physics and M.S. degree in physics of particles from the University of Florence, Florence, in 2011 and 2016, respectively, and Ph.D. degree in information engineering from the University of Florence, Florence, Italy in 2020. He is the recipient of "Florence University Press Award 2020" for the 7 best PhD theses defended at the University of Florence.

Since 2023, he has been a Researcher with the Department of Information Engineering. His research interests include ground penetrating radar, radar interferometry, ground-based radar, and ground-based synthetic aperture radar.

ALESSANDRA BENI (Member IEEE) received the B.S. degree in physics and the M.S. degree in theoretical physics, from the University of Firenze, in 2016 and 2019, respectively. She attended the PhD program in Information Engineering of the University of Firenze from 2020 to 2023.

She is currently with the Department of Information Engineering, University of Firenze, with Post-Doc position. Her research interests include ground-penetrating radar, ground-based synthetic aperture radar, radar interferometry, radar data processing and UAS-based radars.

LUCA BIGAZZI was born in Florence, Italy, in 1987. He received the B.S. degree in electronics engineering and the M.S. degree in electrical and automation engineering, from the University of Florence, in 2013 and 2017, respectively, and Ph.D. degree in information engineering from the University of Florence, Florence, Italy in 2021.

He is currently with the Department of Information Engineering, University of Florence, with a Post-Doc position. His research interests include computer vision, sensor fusion, control systems, robotics, and autonomous navigation.

MASSIMILIANO PIERACCINI (Member IEEE) received the B.S. degree in mechanical engineering from National Chung Cheng University, Chiayi, Taiwan, in Massimiliano Pieraccini received the M.S. degrees in Physics in 1994 and the Ph.D. degree in Non-destructive Testing in 1998 from the University of Florence, Firenze, Italy.

He was a Research Assistant and Associate Professor with Department of Electronics and Telecommunications (former Department of Electronic Engineering) at the University of Florence, Firenze, Italy. Since 2021, he has been a Full Professor with the same Department (now Department of Information Engineering). Currently, he is President of Electronic Engineering School of the University of Florence, Firenze, Italy. Prof. Pieraccini is the author of more than 180 publications, and more than 9 patented inventions. His research interests include ground penetrating radar, ground-based synthetic aperture radar, interferometric radar, microwave sensors.